3-10-2016

Pressure-induced structural transition in copper pyrazine dinitrate and implications for quantum magnetism

Kenneth Robert O'Neal
koneal5@vols.utk.edu

J Zhou
Virginia Commonwealth University

J G. Cherian
University of Tennessee, Knoxville

M M. Turnbull
Clark University

C P. Landee
Clark University

See next page for additional authors

Pressure-induced structural transition in copper pyrazine dinitrate and implications for quantum magnetism

K. R. O'Neal,[1] J. Zhou,[2] J. G. Cherian,[1] M. M. Turnbull,[3] C. P. Landee,[3] P. Jena,[2] Z. Liu,[4] and J. L. Musfeldt[1]
[1]*Department of Chemistry, University of Tennessee, Knoxville, Tennessee 37996, USA*
[2]*Department of Physics, Virginia Commonwealth University, Richmond, Virginia 23284, USA*
[3]*Department of Physics and Carlson School of Chemistry, Clark University, Worcester, Massachusetts 01610, USA*
[4]*Geophysical Laboratory, Carnegie Institution of Washington, Washington D.C. 20015, USA*
(Received 21 November 2015; revised manuscript received 8 February 2016; published 10 March 2016)

We combined synchrotron-based infrared and Raman spectroscopies, diamond anvil cell techniques, and first principles calculations to unveil pressure-induced distortions in quasi-one-dimensional $Cu(pyz)(NO_3)_2$. The crossover at 0.7 GPa is local in nature whereas the transition at 5 GPa lowers symmetry from *Pmna* to $P222_1$ and is predicted to slightly increase magnetic dimensionality. Comparison with prior magnetoinfrared results reveals the striking role of out-of-plane bending of the pyrazine ligand, a finding that we discuss in terms of the possibility of using pressure to bias the magnetic quantum critical transition in this classic $S = 1/2$ antiferromagnet.

DOI: 10.1103/PhysRevB.93.104409

One of the fundamental challenges in functional magnetism is to understand quantum phase transitions, a classic example of which is the crossover from the antiferromagnetic to the fully polarized state [1–5]. Standard approaches to this problem often take advantage of molecule-based magnetic materials which are well known to display overall low energy scales, complex phase diagrams due to competing interactions, and soft lattices [6–11]. One consequence is that small perturbations by an external stimulus can drive out-sized property changes. Copper pyrazine dinitrate, $Cu(C_4N_2H_4)(NO_3)_2$ or $Cu(pyz)(NO_3)_2$, is a superb physical realization of an $S = 1/2$ quantum Heisenberg antiferromagnet, and as such, it has provided a platform for foundational investigations of quantum magnetism including magnetic quantum critical transitions, Tomonaga-Luttinger liquid behavior, and geometric frustration [12–21]. While copper pyrazine dinitrate has been widely studied over a range of temperatures and magnetic fields [18–25], almost nothing is known about the properties under pressure [26] despite evidence for spin-lattice coupling in applied magnetic field [21]. As we will show, this is because the critical pressure of $Cu(pyz)(NO_3)_2$ is much higher than previously anticipated [26].

In this paper, we bring together synchrotron-based infrared and Raman spectroscopies, diamond anvil cell techniques, and complementary first principles calculations to unveil spin-lattice coupling in $Cu(pyz)(NO_3)_2$ under compression. We find critical pressures near 0.7 and 5 GPa that are related to nitrate group distortions and reduction of overall crystal symmetry from *Pmna* to $P222_1$, respectively. The vibrational response of $Cu(pyz)(NO_3)_2$ under compression also provides an opportunity to make a detailed comparison with prior magnetoinfrared spectra [21] which reveal local lattice distortions through the quantum phase transition. Strikingly, we find that the out-of-plane pyrazine bending modes that redshift in applied magnetic field are a subset of those that break symmetry under pressure. This commonality provides enhanced opportunities for tuning the properties of this classic $S = 1/2$ antiferromagnet. Although spin-lattice mixing is most easily investigated in soft, low energy scale materials like $Cu(pyz)(NO_3)_2$, similar energy transfer mechanisms are relevant in higher energy scale compounds.

Needle-shaped crystals of $Cu(pyz)(NO_3)_2$ were grown as described previously [13]. A polycrystalline sample was loaded into a diamond anvil cell [Fig. 1(a)] either neat or with a pressure medium [27] and an annealed ruby ball [28]. Infrared measurements (100–4000 cm^{-1}; 1 cm^{-1} resolution, 300 K) employed the high brightness beam at the National Synchrotron Light Source at Brookhaven National Laboratory [29]. Raman scattering (20–3260 cm^{-1}; 0.5 cm^{-1} resolution, 300 K) was carried out with $\lambda = 532$ nm at <1 mW power. For both infrared and Raman spectra, compression is reversible within our sensitivity. Calculations of phase stability and lattice dynamics were carried out with spin-polarized density functional theory with the generalized gradient approximation [30] using the projector augmented wave method [31–33].

Figures 1(b) and 1(c) displays a close-up view of the low frequency infrared spectra of copper pyrazine dinitrate under compression [33]. We track the mode frequencies versus pressure to identify structural transitions as indicated by mode splitting, abrupt frequency shifts, and the appearance or disappearance of various peaks. Examination of the frequency versus pressure trends [Fig. 1(h)] reveals two different transitions. The crossover at 0.7 GPa, designated here as $P_{C,1}$, is marked by the separation of the two nearly degenerate modes at 338 and 340 cm^{-1} that we assign as Cu-NO_3 counter-rotations and Cu-NO_3 shearing, respectively [Figs. 1(e) and 1(f)] [34]. The former has little interchain motion while the latter is a superior probe of interchain interactions. As pressure is applied the chains are forced together until the nitrate groups between the chains eventually come close together around $P_{C,1}$, hindering their interchain displacement. This explains why the upper branch hardens strongly ($\approx$11 cm^{-1}/GPa) whereas the lower branch is nearly unaffected.

Since the pyrazine rings are not involved in this transition, it should be anticipated that the magnetic properties will be unaffected. Indeed, susceptibility measurements up to 1.16 GPa show no sign of a crossover or change in exchange anisotropy [26]. This is quite different from other molecule-based magnets such as $Co[N(CN)_2]_2$ [35] and $CuF_2(H_2O)_2$(3-chloropyridine) [36] that display pressure-induced magnetic crossovers near 1 GPa. The difference is due to the magnetic

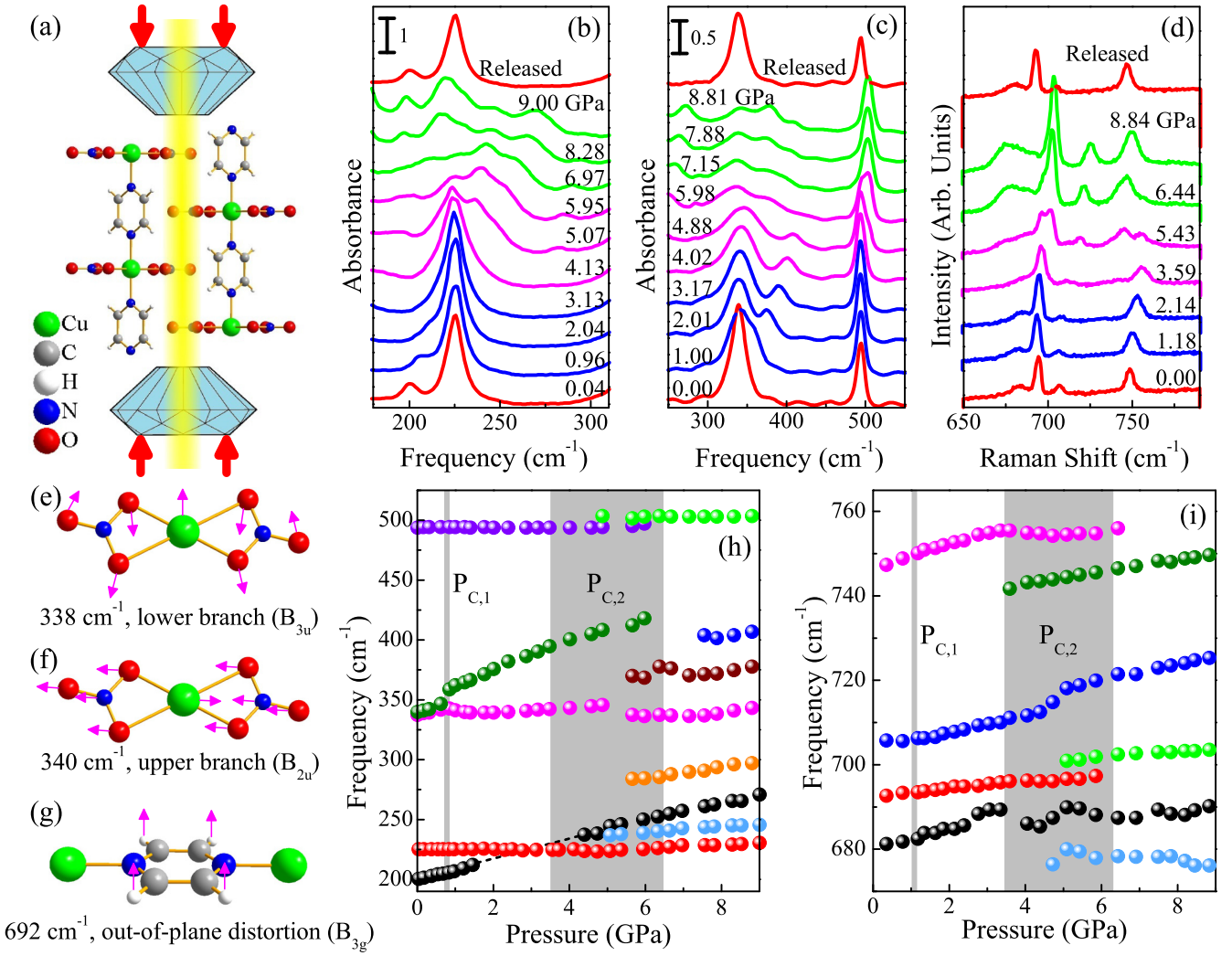

FIG. 1. (a) Schematic representation of the diamond anvil cell used for high pressure vibrational spectroscopy, with the ambient condition structure of $Cu(pyz)(NO_3)_2$ inset between the diamonds. (b),(c) Infrared and (d) Raman spectra under compression and upon release of pressure. Scale bars are included for clarity, and line colors represent different or coexistence of phases. Displacement patterns for the (e),(f) nitrate group modes involved in the 0.7 GPa crossover, and (g) representative out-of-plane pyrazine mode. (h),(i) Frequency versus pressure for the vibrational modes seen in (b)–(d). The gray vertical bands indicate transition regions.

orbitals pointing along the chain direction in $Cu(pyz)(NO_3)_2$ which is not modified through $P_{C,1}$. At the same time, examination of the C-H stretching modes (not shown) reveals no evidence for strengthened hydrogen bonding between the nitrate groups and pyrazine rings, so the rings must be rotating in order to allow the nitrate groups in the neighboring chains to move closer. A small ring rotation may explain the slight decrease in magnetic susceptibility above 0.75 GPa [9,26]. No other infrared- or Raman-active vibrational modes are significantly modified through $P_{C,1}$ indicating that this crossover involves only nitrate groups and is local in nature.

Things are different at higher pressure where a second, more gradual process occurs between 3.5 and 6.5 GPa. This transition, henceforth called the 5 GPa transition and designated as $P_{C,2}$, is broader and associated with phase coexistence [33]. It also involves modes throughout the infrared and Raman spectra—consistent with a space group modification. For instance, nitrate group symmetry is reduced through this transition, as the 340 cm^{-1} Cu-NO_3 shearing mode is blocked and new modes appear [Fig. 1(h)]. The pyrazine ring is also strongly affected as exemplified by the out-of-plane C-H bending mode behavior [Figs. 1(d) and 1(g)]. Overall there are more pyrazine-related vibrational modes observed in the high pressure phase, indicative of lower symmetry due to ring buckling. Cycling tests reveal that spectra before and after compression match very well demonstrating that these local lattice distortions are fully reversible when released from 9 GPa.

The crystal structure above $P_{C,2}$ will naturally be a subgroup of the ambient pressure $Pmna$ space group [37]. Since the pyrazine ring (which is aligned along a) buckles under compression, the symmetry along this axis should be lowered. The most likely subgroup candidates are $Pnc2$ and $P222_1$ as they have reduced a-axis symmetry compared to $Pmna$. In order to distinguish between these possibilities, we analyzed peak splitting as a function of pressure with particular focus

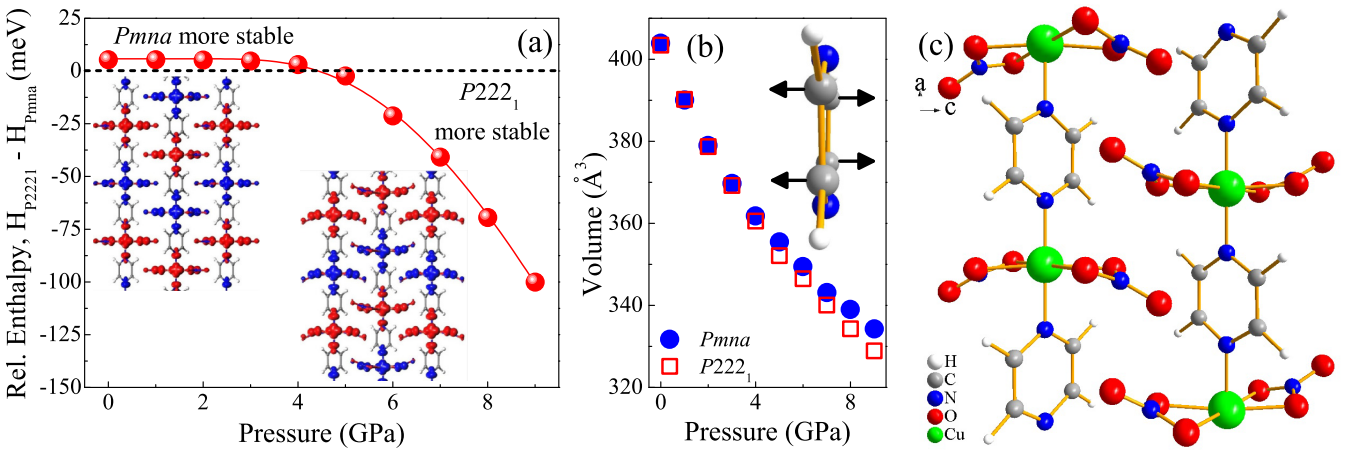

FIG. 2. (a) Relative enthalpy (H = E + PV) and (b) unit cell volume of the ambient *Pmna* and high pressure $P222_1$ phases as a function of pressure. Insets in (a) are calculated magnetic isosurfaces where red and blue surfaces represent spin up and spin down states, respectively. The high pressure state is still a collinear antiferromagnet. The inset in (b) is the calculated high pressure distortions of the pyrazine ring in the indicated directions. (c) Predicted crystal structure of $Cu(pyz)(NO_3)_2$ in the $P222_1$ space group at 10 GPa.

on pyrazine ring and nitrate group behavior. The out-of-plane pyrazine ring distortions through $P_{C,2}$ clearly break symmetry along the *a* axis. The nitrate group also displays a new splitting pattern across the structural transition, as mentioned above. Inspection of the correlation table reveals that *Pnc*2 requires only symmetry lowering along *a* whereas $P222_1$ requires reduced symmetry in all three directions. The latter is therefore the more likely subgroup for the high pressure phase of $Cu(pyz)_2(NO_3)_2$.

For additional tests of phase stability across the pressure-driven structural transition, we constructed models of several different phases of $Cu(pyz)(NO_3)_2$ and performed structural optimizations at various pressures to determine unit cell enthalpy, volume, and magnetic properties [33]. These calculations uncover two stable phases: *Pmna* and $P222_1$. As shown in Fig. 2(a), the enthalpy of the *Pmna* structure is lower than that of $P222_1$ at modest pressures, whereas $P222_1$ becomes more stable above ≈4.5 GPa. This transition pressure agrees very well with the experimentally determined $P_{C,2}$ near 5 GPa. Volume trends [Fig. 2(b)] are also consistent with a transition to $P222_1$ under compression. The predicted crystal structure in the high pressure $P222_1$ phase is shown in Fig. 2(c). Here, the chains shift ≈0.5 Å along the *a* axis, with neighboring chains moving in opposite directions. This brings the NO_3 groups closer together and forces them to bend out of plane [Fig. 2(c)], reducing symmetry in the *bc* plane. The pyrazine rings also display permanent out-of-plane distortions as shown in the inset of panel (b), although they are modest compared to the NO_3 bending. This leads to a symmetry reduction of the ring and thereby the *a* axis. The rings also have a small rotation about *a*, in line with the absence of strengthened hydrogen bonding under pressure.

Assuming that ring distortions and magnetic property changes are commensurate, we anticipate that the magnetic properties of $Cu(pyz)(NO_3)_2$ will start to change only around 5 GPa. The pressure-induced out-of-plane ring distortions modify bond lengths and angles altering the magnetic orbital overlap and reducing *J* as t^2/U [21,38] which, in turn, is expected to weaken intrachain antiferromagnetic ordering. Pressure effects on interchain coupling are, however, still unknown—although decreasing volume generally favors improved exchange interactions. That said, the absence of improved interchain hydrogen bonding under pressure rules out any hydrogen bonding-driven magnetic exchange network dimensionality crossover of the type seen in $CuF_2(H_2O)_2$(pyrazine) [26] or $CuF_2(H_2O)_2$(3-chloropyridine) [36]—at least in this pressure regime. We therefore conclude that the overall trend in the 107 mK ordering temperature in $Cu(pyz)(NO_3)_2$ [19] will depend upon the relative importance of ring distortion vs volume effects. As a point of comparison, we note that pressure elevates T_N and T_C in several other molecule-based materials [35,39–41], although T_N decreases in $Cu(pyz)_2(ClO_4)_2$ [42]. In order to support these hypotheses, we used the calculated high pressure structure to predict the magnetic properties of the $P222_1$ phase. We find similar antiferromagnetic character as evidenced by the out-of-phase spin density pattern [insets, Fig. 2(a)].

One of the major advantages of materials like $Cu(pyz)(NO_3)_2$ is their overall low energy scales compared to cuprates. From the magnetic properties point of view, these compounds can be saturated in experimentally available magnetic fields [6,43,44], providing a superb platform for the study of quantum phase transitions. $Cu(pyz)(NO_3)_2$ is well known to display a magnetic quantum critical transition at 15 T [18]. Here, applied field drives an antiferromagnetic → fully polarized state transition that is facilitated by spin-lattice interactions (which lower J_{AFM} and help to stabilize the fully polarized state) [21,45].

What links the high pressure work presented here with prior magnetoinfrared spectroscopy [21] is the fact that the modes which couple to the field-driven quantum critical transition are the same out-of-plane pyrazine bends that are involved in the 5 GPa structural transition. Figure 3 summarizes this behavior. This similarity is interesting because of the different coupling mechanisms: Pressure acts directly on bond lengths and angles to tune magnetism [38] whereas spin-lattice coupling across the magnetic quantum critical transition relies on spin-orbit effects to link structure and magnetism. As shown in Fig. 3(a),

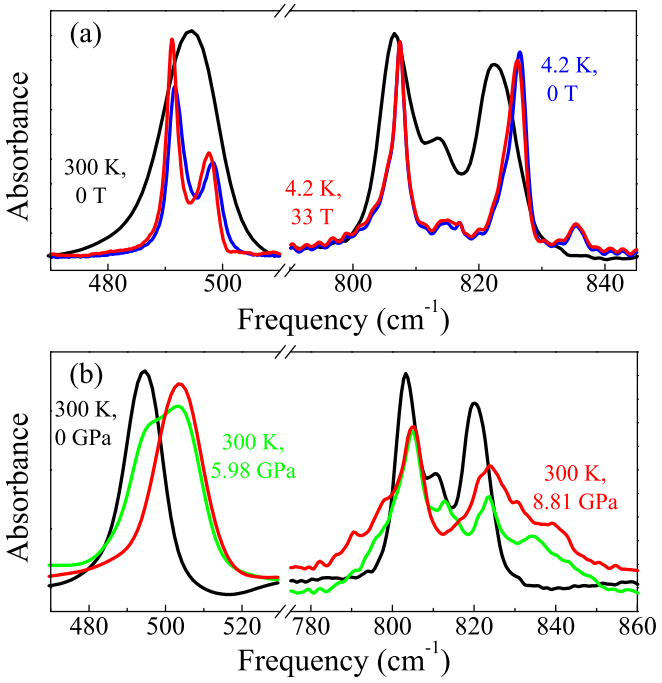

FIG. 3. Close-up views of the infrared response of $Cu(pyz)(NO_3)_2$ in the vicinity of the infrared-active pyrazine ring out-of-plane distortion modes. Panel (a) summarizes the magnetic field-driven changes in these modes (reproduced from Ref. [21]), and (b) brings together complementary high pressure spectra. The conditions for each spectrum are indicated by labels with matching colors.

the out-of-plane bending modes soften through the 15 T transition. The size of this simple redshift follows the square of the magnetization [21] – a clear signature of spin-lattice coupling. Pressure is different. The N out-of-plane bending mode near 490 cm^{-1} splits under pressure, with one branch diminishing while the other grows. Moreover, the cluster of peaks centered near 810 cm^{-1} (assigned as H out-of-plane bends on the ring) blueshift and split into a fivefold multiplet. We conclude that while softening of the out-of-plane ring bends under applied field is small, symmetry is significantly lowered under compression.

What is fascinating is that both types of external stimuli modulate the out-of-plane pyrazine displacements in $Cu(pyz)(NO_3)_2$. It is well known that the pyrazine ring mediates magnetic exchange between copper centers [18], so there may be interesting opportunities to link the mechanisms of magnetic field and pressure driven transitions in this $S = 1/2$ Heisenberg antiferromagnet. The commonality of key displacement patterns under different types of physical tuning, revealed here in copper pyrazine dinitrate, may be present in other molecule-based materials and is associated with the presence of soft ligands that act as superexchange pathways. In fact, recent work by Ghannadzadeh *et al.* demonstrates that magnetic dimensionality and even the critical field is tunable under pressure in a chemically-similar molecule-based magnet that also incorporates pyrazine ligands [26]. This suggests that pressure may be able to bias the quantum phase transition in $Cu(pyz)(NO_3)_2$ as well.

In summary, we measured the vibrational properties of copper pyrazine dinitrate up to 9 GPa in order to explore local lattice distortions in a quasi-one-dimensional $S = 1/2$ quantum Heisenberg antiferromagnet. The structural transition centered at $P_{C,2} = 5$ GPa results in a lower symmetry space group ($P222_1$) under pressure. The energy scale for magnetic property changes is therefore much higher than previously explored. At the same time, comparison of the behavior of the pyrazine out-of-plane distortion modes under pressure to that under magnetic field reveals that incorporating soft ligands as magnetic superexchange pathways can lead to enhanced tunability. In addition to advancing the understanding of spin-lattice coupling in molecule-based materials, this paper emphasizes the advantage of combining pressure and magnetic field to bias the properties of quantum magnets.

This research is funded by the National Science Foundation (DMR-1063880) and the Petroleum Research Fund (52052-ND10). The National Synchrotron Light Source at Brookhaven National Laboratory is supported by the U.S. Department of Energy under Contracts DE-AC98-06CH10886 and DE-FG02-96ER45579. The use of U2A beamline is funded by COMPRES under NSF Cooperative Agreement EAR 11-57758 and CDAC (DE-FC03-03N00144). Resources of the National Energy Research Scientific Computing Center supported by the Office of Science of the U.S. Department of Energy under Contract DE-AC02-05CH11231 are also acknowledged.

[1] S. Sachdev, Nat. Phys. **4**, 173 (2008).
[2] I. A. Zaliznyak, Nat. Mater. **4**, 273 (2005).
[3] N. Büttgen, H.-A. Krug von Nidda, W. Kraetschmer, A. Günther, S. Widmann, S. Riegg, A. Krimmel, and A. Loidl, J. Low Temp. Phys. **161**, 148 (2010).
[4] S. Paschen and J. Lerrea J., J. Phys. Soc. Jpn. **83**, 061004 (2014).
[5] V. Zapf, M. Jaime, and C. D. Batista, Rev. Mod. Phys. **86**, 563 (2014).
[6] P. A. Goddard, J. Singleton, P. Sengupta, R. D. McDonald, T. Lancaster, S. J. Blundell, F. L. Pratt, S. Cox, N. Harrison, J. L. Manson, H. I. Southerland, and J. A. Schlueter, New J. Phys. **10**, 083025 (2008).
[7] Z. Honda, H. Asakawa, and K. Katsumata, Phys. Rev. Lett. **81**, 2566 (1998).
[8] C. P. Landee and M. M. Turnbull, Mol. Cryst. Liq. Cryst. **335**, 193 (1999).
[9] J. L. Manson, S. H. Lapidus, P. W. Stephens, P. K. Peterson, K. E. Carreiro, H. I. Southerland, T. Lancaster, S. J. Blundell, A. J. Steele, P. A. Goddard, F. L. Pratt, J. Singleton, Y. Kohama, R. D. McDonald, R. E. Del Sesto, N. A. Smith, J. Bendix, S. A. Zvyagin, J. Kang, C. Lee, M.-H. Whangbo, V. S. Zapf, and A. Plonczak, Inorg. Chem. **50**, 5990 (2010).
[10] T. V. Brinzari, P. Chen, Q.-C. Sun, J. Liu, L.-C. Tung, Y. Wang, J. A. Schlueter, J. Singleton, J. L. Manson, M.-H. Whangbo,

A. P. Litvinchuk, and J. L. Musfeldt, Phys. Rev. Lett. **110**, 237202 (2013).
[11] T. Lancaster, P. A. Goddard, S. J. Blundell, F. R. Foronda, S. Ghannadzadeh, J. J. Möller, P. J. Baker, F. L. Pratt, C. Baines, L. Huang, J. Wosnitza, R. D. McDonald, K. A. Modic, J. Singleton, C. V. Topping, T. A. W. Beale, F. Xiao, J. A. Schlueter, A. M. Barton, R. D. Cabrera, K. E. Carreiro, H. E. Tran, and J. L. Manson, Phys. Rev. Lett. **112**, 207201 (2014).
[12] R. B. Griffiths, Phys. Rev. **133**, A768 (1964).
[13] A. Santoro, A. D. Mighell, and C. W. Reimann, Acta Crystallogr. **B26**, 979 (1970).
[14] M. B. Stone, D. H. Reich, C. Broholm, K. Lefmann, C. Rischel, C. P. Landee, and M. M. Turnbull, Phys. Rev. Lett. **91**, 037205 (2003).
[15] H. Kühne, H.-H. Klauss, S. Grossjohann, W. Brenig, F. J. Litterst, A. P. Reyes, P. L. Kuhns, M. M. Turnbull, and C. P. Landee, Phys. Rev. B **80**, 045110 (2009).
[16] H. Kühne, A. A. Zvyagin, M. Günther, A. P. Reyes, P. L. Kuhns, M. M. Turnbull, C. P. Landee, and H.-H. Klauss, Phys. Rev. B **83**, 100407 (2011).
[17] Y. Kono, T. Sakakibara, C. P. Aoyama, C. Hotta, M. M. Turnbull, C. P. Landee, and Y. Takano, Phys. Rev. Lett. **114**, 037202 (2015).
[18] P. R. Hammar, M. B. Stone, D. H. Reich, C. Broholm, P. J. Gibson, M. M. Turnbull, C. P. Landee, and M. Oshikawa, Phys. Rev. B **59**, 1008 (1999).
[19] T. Lancaster, S. J. Blundell, M. L. Brooks, P. J. Baker, F. L. Pratt, J. L. Manson, C. P. Landee, and C. Baines, Phys. Rev. B **73**, 020410(R) (2006).
[20] A. A. Validov, M. Ozerov, J. Wosnitza, S. A. Zvyagin, M. M. Turnbull, C. P. Landee, and G. B. Teitel'baum, J. Phys.: Condens. Matter **26**, 026003 (2014).
[21] Ö. Günaydın-Şen, C. Lee, L. C. Tung, P. Chen, M. M. Turnbull, C. P. Landee, Y. J. Wang, M.-H. Whangbo, and J. L. Musfeldt, Phys. Rev. B **81**, 104307 (2010).
[22] B. R. Jones, P. A. Varughese, I. Olejniczak, J. M. Pigos, J. L. Musfeldt, C. P. Landee, M. M. Turnbull, and G. L. Carr, Chem. Mater. **13**, 2127 (2001).
[23] A. V. Sologubenko, K. Berggold, T. Lorenz, A. Rosch, E. Shimshoni, M. D. Phillips, and M. M. Turnbull, Phys. Rev. Lett. **98**, 107201 (2007).
[24] J. Rorhkamp, M. D. Phillips, M. M. Turnbull, and T. Lorenz, J. Phys. Conf. Ser. **200**, 012169 (2010).
[25] J. Jornet-Somoza, M. Deumal, M. A. Robb, C. P. Landee, M. M. Turnbull, R. Feyerherm, and J. J. Novoa, Inorg. Chem. **49**, 1750 (2010).
[26] S. Ghannadzadeh, J. S. Möller, P. A. Goddard, T. Lancaster, F. Xiao, S. J. Blundell, A. Maisuradze, R. Khasanov, J. L. Manson, S. W. Tozer, D. Graf, and J. A. Schlueter, Phys. Rev. B **87**, 241102(R) (2013).
[27] Neat for Raman, vacuum grease for far infrared, and KBr for middle infrared. These media ensure that the applied pressure is continuous, three-dimensional, and quasihydrostatic.
[28] H. K. Mao, P. M. Bell, J. W. Shaner, and D. J. Steinberg, J. Appl. Phys. **49**, 3276 (1978).
[29] G. L. Carr, M. C. Martin, W. R. McKinney, K. Jordan, G. R. Neil, and G. P. Williams, Nature London) **420**, 153 (2002).
[30] J. P. Perdew, K. Burke, and M. Ernzerhof, Phys. Rev. Lett. **77**, 3865 (1996).
[31] P. E. Blöchl, Phys. Rev. B **50**, 17953 (1994).
[32] G. Kresse and J. Furthmüller, Phys. Rev. B **54**, 11169 (1996).
[33] See Supplemental Material at http://link.aps.org/supplemental/10.1103/PhysRevB.93.104409 for more details.
[34] P. M. Castro and P. W. Jagodzinski, J. Phys. Chem. **96**, 5296 (1992).
[35] C. J. Nutall, T. Takenobu, Y. Iwasa, and M. Kurmoo, Mol. Cryst. Liq. Cryst. **343**, 227 (2000).
[36] K. R. O'Neal, T. V. Brinzari, J. B. Wright, C. Ma, S. Giri, J. A. Schlueter, Q. Wang, P. Jena, Z. Liu, and J. L. Musfeldt, Sci. Rep. **4**, 6054 (2014).
[37] This symmetry analysis assumes that the transition is second order.
[38] J. B. Goodenough, *Magnetism and the Chemical Bond* (Wiley, New York, 1963).
[39] J. J. Hamlin, B. R. Beckett, T. Tomita, J. S. Schilling, W. S. Tyree, and G. T. Yee, Polyhedron **22**, 2249 (2003).
[40] M. Mito, J. Phys. Soc. Jpn. **76**, 182 (2007).
[41] P. A. Quintero, D. Rajan, M. K. Peprah, T. V. Brinzari, R. S. Fishman, D. R. Talham, and M. W. Meisel, Phys. Rev. B **91**, 014439 (2015).
[42] N. Barbero, T. Shiroka, C. P. Landee, M. Pikulski, H.-R. Ott, and J. Mesot, Phys. Rev. B **93**, 054425 (2016).
[43] A. Orendáčová, E. Čižmár, L. Sedláková, J. Hanko, M. Kajňaková, M. Orendáč, A. Feher, J. S. Xia, L. Yin, D. M. Pajerowski, M. W. Meisel, V. Zeleňák, S. Zvyagin, and J. Wosnitza, Phys. Rev. B **80**, 144418 (2009).
[44] P. Vrábel, M. Orendáč, A. Orendáčová, E. Čižmár, R. Tarasenko, S. Zvyagin, J. Wosnitza, J. Prokleška, V. Sechovský, V. Pavlík, and S. Gao, J. Phys.: Condens. Matter **25**, 186003 (2013).
[45] J. L. Musfeldt, L. I. Vergara, T. V. Brinzari, C. Lee, L. C. Tung, J. Kang, Y. J. Wang, J. A. Schlueter, J. L. Manson, and M.-H. Whangbo, Phys. Rev. Lett. **103**, 157401 (2009).

Supplementary material for "Pressure-induced structural transition in copper pyrazine dinitrate and implications for quantum magnetism"

K. R. O'Neal,[1] J. Zhou,[2] J. G. Cherian,[1] M. M. Turnbull,[3]
C. P. Landee,[3] P. Jena,[2] Z. Liu,[4] and J. L. Musfeldt[1]

[1]*Department of Chemistry, University of Tennessee, Knoxville, Tennessee 37996, USA*

[2]*Department of Physics, Virginia Commonwealth University, Richmond, Virginia 23284, USA*

[3]*Department of Physics and Carlson School of Chemistry, Clark University, Worcester, Massachusetts 01610, USA*

[4]*Geophysical Laboratory, Carnegie Institution of Washington, Washington D.C. 20015 USA*

Ambient condition vibrational response

Copper pyrazine dinitrate, or $Cu(pyz)(NO_3)_2$, displays a rich infrared spectrum (Fig. S1 (a)) with over 100 vibrational features including fundamental, combination, and overtone modes [S1, S2]. The same is true for the Raman spectrum (Fig. S1 (b)), although it has not been previously reported. We therefore provide mode assignments for both the infrared- and Raman-active fundamental modes (Tables S1 and S2, respectively). We limited our high pressure spectra to $\sim$3200 cm^{-1} in order to avoid the overtone and combination modes, simplifying the analysis [S1, S2].

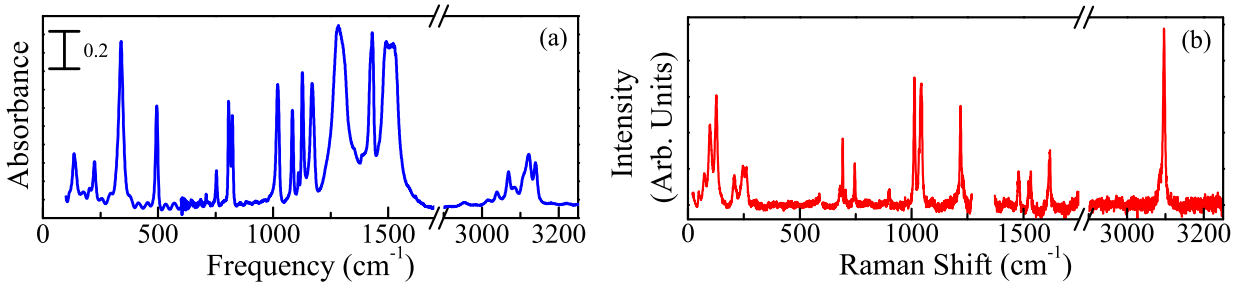

FIG. S1: Ambient condition (a) infrared and (b) Raman spectra of copper pyrazine dinitrate. Regions corresponding to diamond absorption or displaying no features are omitted for simplicity. Scale bars are included for clarity.

TABLE S1: Assignment of the infrared modes for $Cu(pyz)(NO_3)_2$ at ambient conditions.

Frequency (cm^{-1})	Mode displacement pattern
95	Cu motion with in-plane pyz and NO_3 counter-rotations
135	Cu motion along a with NO_3 in-phase, out-of-plane rocking about outermost O
200	Cu motion with pyz in-plane rotation with in-plane Cu-NO_3 rotation
225	Cu motion along a axis
338	Cu-NO_3 in-plane counter-rotation
340	Cu-NO_3 shearing
494	pyz out-of-plane N displacement
752, 805, 813, 822	pyz out-of-plane C-H wags
1016 - 1165	pyz in-plane bends, stretches
1282	NO_3 group N in-plane motion
1381, 1425, 1428	pyz in-plane C-H wags
1488	pyz out-of-plane C-H wag
1519	pyz C=C-N asymmetric stretch
2951 - 3135	C-H stretches

TABLE S2: Assignment of the Raman modes for $Cu(pyz)(NO_3)_2$ at ambient conditions.

Frequency (cm^{-1})	Mode displacement pattern
48	Cu motion with pyz flapping
74	pyz twist about a axis
98	out-of-phase, out-of-plane NO_3 rocking about outermost O
127	NO_3 out-of-plane rotation
207	pyz out-of-plane rotation
248	(NO_3)-Cu-(NO_3) symmetric stretch, no Cu motion
260	(NO_3) in-plane rotation
681, 692, 705, 747	pyz out-of-plane C-H wags
1013, 1043	pyz in-plane bends, stretches
1218, 1479	pyz out-of-plane C-H wag
1523	symmetric C=N=C stretch
1533	asymmetric C=N=C stretch
1614, 1618	pyz N displacement
3087, 3098	C-H stretch

Low frequency modes

While the ligand modes discussed in the main text reveal local lattice distortions through the 0.7 and 5 GPa transitions, the low frequency modes (Fig. S2) are also important. These modes show no changes through the 0.7 GPa transition, confirming that it involves only the nitrate groups. We caution that the infrared mode near 100 cm^{-1} is not appearing at $P_{C,1}$ but

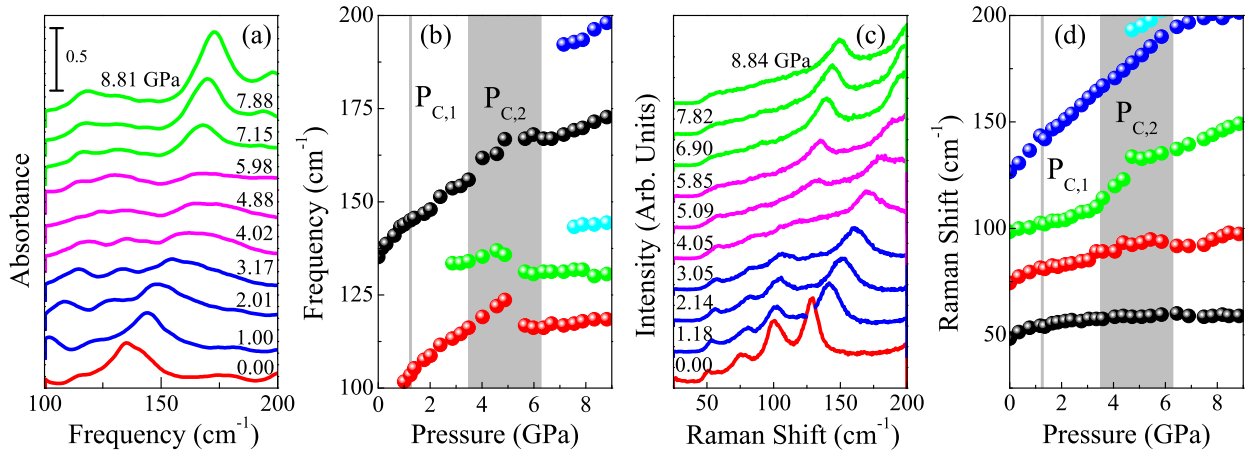

FIG. S2: Close-up view of the low frequency (a) infrared and (c) Raman spectra of $Cu(pyz)(NO_3)_2$ under compression. Pressures are indicated, scale bars are included for clarity, and line colors correspond to different or coexisting phases. Red corresponds to the ambient *Pmna* structure, blue represents the structure above $P_{C,1}$, pink is the crossover region where two phases coexist, and green is the predicted $P222_1$ phase above $P_{C,2}$. Frequency versus pressure for the (b) infrared- and (d) Raman-active modes. Gray vertical lines represent transition regions.

coincidentally moving into our experimental frequency range. There are several signatures of the 5 GPa transition. For instance, the lowest frequency infrared-active mode shows a discontinuity and slope change along with symmetry breaking evidenced by the appearance of new peaks at 135 and 145 cm^{-1}. The 100 cm^{-1} Raman-active mode also displays a cusp-like frequency shift through $P_{C,2}$. The highly collective nature of these modes makes it challenging to correlate specific displacement patterns to the symmetry breaking. That these features change through $P_{C,2}$ is, however, consistent with an overall symmetry reduction to $P222_1$ at high pressure.

Phase coexistence between 3.5 and 6.5 GPa

The higher pressure transition discussed in the main text takes place over a broad pressure region (3.5 to 6.5 GPa). Within this range there is a gradual crossover to a new structure. This can be seen, for instance, in the behavior of the out-of-plane bending mode of pyrazine shown in Fig. S3. Only one peak is observed below $P_{C,2}$. As pressure is applied a new mode at slightly higher frequency begins to gain intensity. At 5.66 GPa, the two branches have

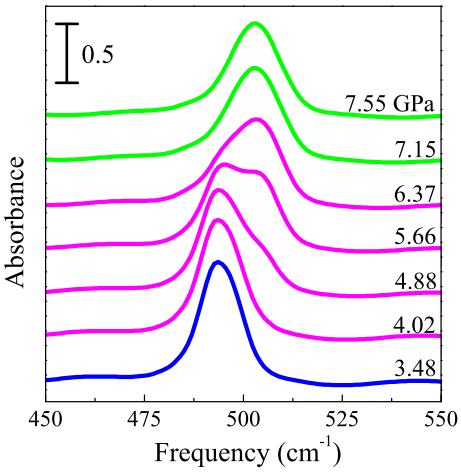

FIG. S3: Close-up view of the infrared-active pyrazine out-of-plane mode of $Cu(pyz)(NO_3)_2$ at the indicated pressures displaying the coexistence of phases between about 3.5 and 6.5 GPa. Line colors correspond to different or coexisting phases using the same scheme as Fig. S2. A scale bar is included for clarity.

similar intensities, indicating that half of the material is in the low pressure structure and the other half is in the new, high pressure phase. Above this pressure, the lower frequency peak diminishes until the structural transition is complete around 6.5 GPa and only the high frequency mode remains.

Computational details, high pressure structure, and magnetic properties

Calculations of phase stability were performed with spin-polarized density functional theory with the generalized gradient approximation treatment for the exchange-correlation functional [S3] using the projector augmented wave method [S4] as implemented in the Vienna *ab initio* simulation package [S5]. A plane wave energy cutoff of 520 eV and Monkhorst-Pack k point meshes [S6] of (4×4×3) were adopted. The convergence threshold for total energy was set at 10^{-4} eV. Calculations were carried out for a unit cell containing two copper centers. The geometric structures were relaxed using the conjugated gradient method without any symmetry constraints until the Hellman-Feynman force on each atom was smaller than 0.01 eV/Å. Grimme's method was used for van der Waals interaction corrections [S7].

As discussed in the main text, our spectral analysis suggests that the high pressure phase of copper pyrazine dinitrate should adopt the $P222_1$ space group. We therefore wanted to carry out calculations to verify this supposition. There is, however, no way to thoroughly predict an unknown structure, so various possibilities were tested. In our set of calculations, the ambient *Pmna* structure was artificially perturbed resulting in structures with different space groups (e.g. *Pnc*2 and $P222_1$). These perturbations cover the two most likely

possibilities. We then applied density functional theory along with structural optimization calculations at different pressures to see how these candidates respond. If after structural optimization a structure went back to *Pmna*, it was considered to be unstable. On the other hand, if a structure went to a space group other than *Pmna*, then it is a local energy minimum. We find that only the $P222_1$ structure is a local minima, while all other candidates revert to the *Pmna* phase. The energy and volume for the *Pmna* and $P222_1$ phases were calculated at various pressures up to 10 GPa (Fig. 3, main text).

We also calculated the magnetic properties of the anticipated high pressure ($P222_1$) phase of copper pyrazine dinitrate using spin-polarized density functional theory. The inter-chain magnetic coupling is computed by taking the energy difference of ferromagnetic ($E_{1,FM}$) and antiferromagnetic ($E_{1,AFM}$) states of the simulating supercell described above. According to the Ising model, $E_{1,FM} = -2JS^2$ and $E_{2,AFM} = 2JS^2$. Here, the factor 2 indicates two couplings within one supercell. Hence, $J = (E_{1,FM} - E_{1,AFM})/4S^2$. In order to calculate the intra-chain coupling, we double the simulating supercell along its z direction, and calculate the $E_{2,FM}$ and $E_{2,AFM}$, and the coupling is $J = (E_{2,FM} - E_{2,AFM})/4S^2$. We find that each copper center carries $\approx 1\ \mu_B$ magnetic moment and favors a collinear antiferromagnetic arrangement. However, the magnetism around Cu is not highly localized. The out-of-phase spin density pattern characteristic of antiferromagnetism is shown in Fig. 3(a) in the main text, which shows that the NO_3 ligands are also spin polarized by the Cu. We also included spin-orbital coupling to examine possible magnetocrystalline anisotropy of the copper atoms. A very low value was obtained (less than 0.3 meV).

[S1] B. R. Jones, P. A. Verughese, I. Olejniczak, J. M. Pigos, J. L. Musfeldt, C. P. Landee, M. M. Turnbull, and G. L. Carr, Chem. Mater. **13**, 2127 (2001).

[S2] S. Brown, J. Cao, J. L. Musfeldt, M. M. Conner, A. C. McConnell, H. I. Southerland, J. L. Manson, J. A. Schlueter, M. D. Phillips, M. M. Turnbull, and C. P. Landee, Inorg. Chem. **46**, 8577 (2007).

[S3] J. P. Perdew, K. Burke, and M. Ernzerhof, Phys. Rev. Lett. **77**, 3865 (1996).

[S4] P. E. Blöchl, Phys. Rev. B **50**, 17953 (1994).

[S5] G. Kresse and J. Furthmüller, Phys. Rev. B **54**, 11169 (1996).

[S6] H. J. Monkhorst and J. D. Pack, Phys. Rev. B **13**, 5188 (1976).

[S7] S. Grimme, J. Comput. Chem. **27**, 1787 (2006).